Creating Three-Dimensional Polymeric Microstructures by Multi-Beam Interference Lithography

Jun Hyuk Moon and Shu Yang[1]

Department of Materials Science and Engineering, University of Pennsylvania, 3231 Walnut Street, Philadelphia, PA 19104, USA

[1] Correspondence: S. Yang, Department of Materials Science and Engineering, University of Pennsylvania, 3231 Walnut Street, Philadelphia, PA 19104, USA.
Email: shuyang@seas.upenn.edu

CONTENTS

Abstract

It is attractive to produce true three-dimensional (3D) microstructures both rapidly and economically over a large area with negligible defects for a wide range of applications. Multi-beam interference lithography is one of the promising techniques that can create periodic microstructures in polymers without extensive lithography and etching steps. This review discusses the formation of interference patterns, their dependence on beam parameters, the lithographic process, and the applications to the formation of photonic crystals. Various photoresist systems, including thick films of negative-tone and positive-tone photoresists, liquid resins, organic-inorganic hybrids, and holographic polymer-dispersed liquid crystals, are also reviewed.

Key words: multi-beam Interference, lithography, 2D and 3D microstructures, maskless, photoresist, negative-tone, positive-tone, organic-inorganic hybrids, and holographic polymer-dispersed liquid crystals

1. Introduction

Recent enthusiasm in photonics(1), chemical sensors(2), catalytic support(3), data storage(4), nano- and microfludic networks(5), and tissue engineering(6-8) has driven the development of new materials and tools for the creation of structures with tailored functionalities, shapes and sizes. Although major progress has been made in the fabrication of two-dimensional (2D) structures, significant challenges remain for rapid, inexpensive, and large area fabrication of true three-dimensional (3D) structured materials with submicron periodicity and with negligible defect densities. Existing techniques for the large-scale fabrication of microstructures with submicron features mainly rely on the use of optical projection lithography developed for silicon IC manufacturing. This method is inherently limited to 2D patterning and requires laborious layer-by-layer photolithography and etching processes to generate the continuous 3D structures.(9-12) A set of different chrome masks is required to form each of the different layers using conventional projection lithography. (13) The masks for the lithographic processes are expensive to fabricate and therefore, mask costs can be a significant portion of the total cost for the multi-level fabrication process of microstructures. Furthermore, precise optical systems with vertical and horizontal steppers are required for repositioning and registration. The fabrication is thus practical only up to a few layers.

Self-assembly approaches, such as crystallization of colloidal particles(14,15), microphase separation of block copolymers(16) are simple and inexpensive. Recently there have been extensive studies using templates and external fields,(17-21) to minimize random defects, however, intrinsic problems, such as missing particles, uncontrolled

orientation, phase mixing, and dislocations, are inevitable over a large area. In addition, the type of lattice created from colloidal assembly is rather limited, typically exhibiting face-centered-cubic (fcc) symmetry. Other 3D microfabrication techniques, including three-axis micropositioner assisted deposition of polymer melts and solutions (e.g. rapid prototyping(22,23), pressure assisted microsyringe deposition(24), focused-ion-beam etching(25), and direct-write assembly(26,27), etc.), layer-by-layer stacking through soft lithography(28), glancing angle deposition (GLAD)(29), and multi-photon absorption at near-IR (4,30-35), requires *multiple steps* to create 3D microstructures of almost arbitrary complexity.

In comparison, multi-beam interference lithography, which is based on the optical patterning of photopolymers in a *single exposure* (a few nanoseconds to seconds), holds promise for the rapid production of highly ordered 2D and 3D structures with submicron periodicity defect-free over a large area. It allows for precise control of the size and shape of the resulting structures, and has the flexibility to access a variety of lattice symmetries through proper arrangement of laser beams. It has been demonstrated for various applications, including photonic crystals(36-43), microlens arrays(44), information storage(45), and optical communication.(46,47) Furthermore, it is compatible with multi-photon lithography technique, which relies on similar photochemistry to pattern arbitrary structures in polymers. The integration of multi-beam interference lithography and 2-photon lithography will enable fast production of 3D structures with controlled, functional elements (e.g. cavity defects and waveguides) *in situ* through sequential exposures to multi-photon and interference beams, or *vice versa*.

A detailed comparison of the fabrication capabilities and resolution limits of different techniques are summarized in Table 1.

A. Conventional photolithography(48)

In a conventional photolithographic process, a photoresist that contains photoinitiators, photosensitive resin and additives (e.g., radical scavengers, bases or dissolution inhibitors) are spin coated on a substrate and baked to remove the solvent. It is flood-exposed through a mask under a light source, resulting in 2D patterns. (Scheme 1) Depending on the products generated during photoexposure, radicals or cations, the photosensitive resin can be either polymerized/crosslinked or decomposed, resulting in solubility change from the starting medium in a developing solvent. In a negative-tone photoresist, the exposed regions are crosslinked when the intensity of the interference pattern exceeds the lithographic threshold of the photoresists. The unexposed regions are washed away by a developer (typically an organic solvent), resulting in a porous film. The threshold intensity is determined by the sensitivity of the photoresist and post-exposure processing (e.g., baking time and temperature, choice of developers and developing time), as well as the contrast of the interference pattern. In positive-tone photoresists, the exposed regions will be removed by the developer (typically an aqueous base), while the unexposed or weakly exposed regions remain. Currently, most of the thick photoresists are negative-tone. Positive-tone resists may have higher resolution and better contrast since the resists are typically chemically amplified, and have large a polarity change in the aqueous base developer before and after the lithography. In contrast to the dissolution of unpolymerized oligomers in negative-tone resists, the

solubility switch in positive-tone resists is due to the polarity change of the side groups, thus, films from positive-tone resists will have much less shrinkage and delamination in comparison to that from negative-tone resists.

The maximum resolution is determined by the efficiency of photochemistry, the exposure wavelength, and the resolution of optics. When feature size continues to shrink on integrated chip (IC) devices, it becomes increasingly demanding to materials scientists for innovations in photoresist design and fabrication, such as maximizing photospeed while maintaining high film transparency at shorter wavelengths. Detailed review on conventional lithography can be found elsewhere.(48)

B. Multi-beam interference lithography

When two or more optical waves are present simultaneously in the same region of space, the waves interfere and generate a periodic spatial modulation of light(49). Interference among any N (≤4) collimated, coherent laser beams produces an intensity grating with (N-1) dimensional periodicity if the difference between the wave vectors is non-coplanar. As shown in Fig 1, two interfering beams form a 1D fringe pattern (Fig. 1a) and three crossed beams form a 2D hexagonal pattern (Fig. 1b).

The intensity distribution of the interference field can be described by a Fourier superposition as the following:

$$I = \sum_{i=1}^{N} \left|\mathbf{E}_i\right|^2 + \sum_{i>j=1}^{N} \mathbf{E}_i^* \cdot \mathbf{E}_j \exp[i\{(\mathbf{k}_j - \mathbf{k}_i)\cdot\mathbf{r} + (\varphi_j - \varphi_i)\}] \qquad (1)$$

where $\mathbf{r}$ is the position vector, $\mathbf{E}_i$, $\mathbf{k}_i$ and φ_i are the complex amplitude, wave vector, and phase of the ith beam, respectively. The difference between two of the wave vectors, $(\mathbf{k}_i - \mathbf{k}_j)$, where $i, j = 1,2, \ldots, N$ and $i<j$, determines the spatial periodicity, or the

translational symmetry of the interference pattern.(50-53) The contrast of interference pattern is controlled by the real amplitude, polarization and phase of each beam. The combination of these parameters determines the overall symmetry and contrast of the resulting lattice.(41,43,54,55)

Multi-beam interference previously was used to write hologram gratings, to create optical traps for laser-cooled atoms(56), and to pattern optical tweezer arrays(57-59) Recently, it has been integrated with lithography to produce periodic structures with sub-micron resolution.(36-40,43) The photochemistry and lithographic processes involved in multi-beam interference are similar to those in the conventional lithography except that photomasks are not required, and the substrate is transparent since all of the beams are not necessarily launched from the same side of the substrate (see Scheme 2).

Because the multiple beams must be coherent to produce an interference pattern, one laser beam from a visible (e.g. Ar-ion, frequency-doubled Nd:YAG, and Nd:YVO_4) or UV (e.g. frequency-tripled Nd:YAG and He-Cd) laser is typically divided into multiple beams using beam-splitters. The split beams are then recombined by mirrors to obtain the desired geometry. The polarization and intensity of the beams are controlled by wave plates and polarizers, respectively. The combined beams are then focused on a relatively thick photoresist film (up to100 μm) for a few nanoseconds to seconds, depending on the resist sensitivity and laser power from a pulsed or a continuous wave (cw) laser.

C. Formation of Two-Dimensional (2D) Microstructures

2D interference patterns can be obtained using different interference techniques,

including interference by three focused beams(60), multiple diffraction grating masks(38,61,62), and double exposures of a two-beam interference.(63,64)

In the first case, the configuration of focused three beams determines the translational symmetry of the 2D pattern. Here we briefly introduce the practical setup for several 2D lattices. As shown in Fig. 2a and 2b, three beams are set to have the same polar angles to the z-axis of an arbitrary xyz-coordinate space, and described as $\mathbf{k}_i = 2\pi/\lambda(\cos\phi_i \sin\theta, \sin\phi_i \sin\theta, \cos\theta)$, for *i*=1,2,3, ,where θ and ϕ_i are the polar and azimuthal angles. The difference between two wave vectors lies within the xy-plane, producing a 2D interference pattern with basis vectors of $\mathbf{b}_1 = (\mathbf{k}_1 - \mathbf{k}_2)$ and $\mathbf{b}_2 = (\mathbf{k}_2 - \mathbf{k}_3)$ in the reciprocal lattice (Fig. 2d). Subsequently, the lattice constants and the angle between basis vectors in real space can be expressed as

$\mathbf{a}_1 = \frac{\lambda}{|\sin\theta(\cos\phi_1 - \cos\phi_2)|}$, $\mathbf{a}_2 = \frac{\lambda}{2|\sin\theta \sin\phi_2 \sin((\phi_1 + \phi_2)/2)|}$, and $\gamma = (\phi_1 + \phi_2)/2$, where λ is the wavelength of the laser (Fig. 2c). The experimental conditions for 2D square and tetragonal lattices are shown in Table 2.(42) Meanwhile, considering linearly polarized beams and no interference between beam 1 and 3 (i.e., $\mathbf{E}_1 \cdot \mathbf{E}_3$=0), the square lattice can be described by

$$I = \sum_{i=1}^{3} |\mathbf{E}_i|^2 + \mathbf{E}_1 \cdot \mathbf{E}_2 \cos[2\pi x/\mathrm{a}] + \mathbf{E}_2 \cdot \mathbf{E}_3 \cos[2\pi y/\mathrm{a}] \quad (2)$$

from Eq. (1). The symmetry of the “atoms” in the “basis” is dependent on the polarization of the beams as shown in Fig. 3 by changing the ratios of $(\mathbf{E}_1 \cdot \mathbf{E}_2)/(\mathbf{E}_2 \cdot \mathbf{E}_3)$.

When a grating mask is used to pattern a photoresist, the incident beam is diffracted by three or four diffraction gratings aligned at an angle to each other.(62,65) The first-order diffracted beams interfere and produce the pattern. Compared to the

three-beam setup, this method is more stable due to the use of a single monolithic diffracting object. Since the interference pattern depends on the period of the gratings and the angle between gratings, different grating masks are required to vary the size of the pattern.

In addition to the two techniques mentioned above, which are based on a single exposure of three beams, 2D patterns can also be obtained through multiple exposures of two-beam interference.(63,66,67) In practice, it is much more convenient to arrange two beams with different geometries to access a wide range of lattices with variable unit sizes and large contrast. For example, both square and tetragonal 2D lattices can be attained by simply rotating the sample stage with a precise control of the in-plane rotation of the substrate.

D. Formation of Three-Dimensional (3D) Microstructures

The ability to rapidly produce periodic microstructures by multi-beam interference lithography defect-free over a large area is particularly attractive for the fabrication of 3D photonic crystals (PCs) in the visible or near-IR telecommunication wavelength (λ of 1.33 and 1.55 μm). A photonic crystal is a regularly structured material with a periodic modulation in refractive index, or dielectric constant, on a length scale comparable to the wavelength of the incident light.(68),(69) Interference of the light waves scattered from the dielectric lattice (*i.e.* Bragg scattering) leads to stop bands or complete photonic band gaps (PBG), which are analogous to the electronic energy bandgaps in a semiconductor.

They can be fabricated using four-beam interference(36,39,40), diffraction grating masks(37), multiple exposure techniques(43,70), and phase masks on a controlled stage.(71) 3D lattices that possess large photonic band gaps, including simple cubic, face-

centered cubic (f.c.c), diamond, body-centered cubic (b.c.c), and gyroid lattices have been demonstrated both theoretically and experimentally.(41,43,72-74) In this review, we will focus on the fabrication of 3D photonic structures.

It has been predicted that the translational symmetries associated with all 14 Bravais lattices can be accessible through multi-beam interference lithography(53), however, little attention has been paid to the effect of the beam polarization on the overall symmetry until recently. As shown in the formation of 2D patterns, the symmetry of the "atoms" in the "basis" will be affected by the beam polarization vectors (Fig. 3). When the polarizations are taken into account, the overall symmetry of the interference pattern may not respect all the required site symmetries of the particular Bravais lattice, or correspond to any one of the space groups of the originally specified Bravais lattice. Clearly, there is a need to establish a better understanding of the relationship between the resulting symmetries and the beam parameters.

A level-set approach has been proposed to equate terms of the intensity equation to a representative level surface of the desired space group.(55) This technique was previously used to describe minimal surfaces in microphase-separated morphologies such as those typically found in the block copolymer systems.(75) In this approach the complete symmetry of the 3D lattice is defined by its structure factors. The level surfaces are functions that are of the form F: $\mathbf{R}^3 \rightarrow \mathbf{R}$ of points $\{x, y, z\} \in \mathbf{R}^3$ that satisfy the equation $F(x, y, z) = t$, where t is a constant. When $F(x,y,z)=0$, it defines a boundary between positive F and negative F. Specifically, a candidate structure can be modeled using a 3D surface given by $F(x,y,z)-t=0$. By varying the value of the constant t, which can be achieved experimentally by adjusting the threshold value of the photoresist(39,76),

we can access a family of surfaces with different volume fractions to tune the photonic band structure. When equating terms of the intensity equation to a level surface, we can calculate the beam parameters (wave vectors, polarizations, intensity, etc.) to construct a desired 3D lattice. For example, the three-termed simple-cubic, diamond-like (fcc translational symmetry) and gyroid-like (bcc translational symmetry) structures have been calculated using the level-set approach (see Table 3).(43) The equations describing these structures are given by

$$F(x, y, z) = \sin(x) + \sin(y) + \sin(z) + t \quad (3)$$

for a simple cubic surface,

$$F(x, y, z) = \sin(-x+y+z) + \sin(x-y+z) + \sin(x+y-z) + t \quad (4)$$

for a diamond-like structure, and

$$F(x, y, z) = \sin(y+z) + \sin(y-z) + \sin(-x+z) + t \quad (5)$$

for a gyroid structure, respectively. The plots of the corresponding isointensity surfaces are shown in Fig. 4.

II. PHOTOSENSITIVE MATERIALS AND THEIR APPLICATIONS

A. Negative-tone Photoresists

To fabricate 3D photonic crystal structures, a thick photoresist film is usually required for a multi-layer unit cell. Negative-tone photoresists, such as SU-8, are commonly used for thick films (thickness up to 2 mm with an aspect ratio approaching 20). SU-8 has high solubility in many organic solvents, which enables the preparation of thick films and it is highly transparent in the near-UV and visible region. Commercially available SU-8 photoresists (Microchem Inc.) consist of EPON SU-8

(from Shell Chemicals), a derivative of bisphenol-A-novolac resin with an average of eight epoxy groups, triaryl sulphonium salts as photoacid generators (PAG)(77) (see Scheme 3), and γ-butyrolactone (GBL) or cyclopentanone (CP) as a solvent. The solution is spun onto a cover glass and baked on a hotplate at 95°C to evaporate the solvent. During UV exposure, the triaryal sulfonium salts release photoacids in localized regions. The subsequent post-exposure bake at 95°C accelerates acid diffusion and induces cationic polymerization of the epoxy groups in SU-8.(78-80) The unexposed film was removed by propylene glycol methyl ether acetate (PGMEA), followed by supercritical CO_2 drying to prevent pattern collapse. The low surface tension of supercritical CO_2 is especially advantageous in removing solvents from films with high porosity and high aspect ratio features. The resulting SU-8 film is highly crosslinked and exhibits excellent thermal ($Tg > 200^{\circ}C$) and mechanical strength (Young's modulus, $E > 4.0$ GPa).

The relatively high glass transition temperature of SU-8 photoresists, 50°C, plays an important role in minimizing acid diffusion before the post-exposure bake. A high glass transition temperature has been one of the key resist design criteria to achieve submicron resolution in deep UV lithography of chemically amplified photoresists. It is equally important in interference lithography since polymerization during exposure is not desired: this would disturb the original interference pattern due to the change of refractive index of the crosslinked film. When the film is exposed at room temperature and then baked at 95°C, the exposure and crosslinking stages are separated.

Although SU-8 resin is quite transparent in the near-UV region, it is more appealing to perform interference lithography using visible light. Not only is the visible

continue wave (cw) laser more readily accessible in the lab than the UV pulsed laser, but a longer wavelength affords a larger lattice period. Further, the transmission of the SU-8 photoresists increases significantly in the visible region, therefore interference of visible light is more flexible and applicable to a wide range of photosensitive materials.

Since most photoacid generators do not have absorption in visible wavelength, the resists are formulated based on visible laser-sensitized cationic polymerization of epoxides.(81,82) This initiating system typically includes a photosensitizer, which absorbs the visible light and electron transfers to an onium salt via the formation of a charge transfer complex to generate the acids (see Scheme 4). Typically diaryliodionium salts are chosen as photoacid generators instead of triarylsulfonium salts due to the low reduction potential of iodionium salts for energy transfer. The photoacids initiate ring-opening reactions of the epoxy groups and the acids are regenerated in the subsequent steps.(83,84) The polymerization is thus chemically amplified, resulting in a highly crosslinked film. Several visible photosensitizer/PAG systems for SU-8 photoresists have been developed, including xanthene dyes, 2,4,5,7-tetraiodo-6-hydroxy-3-fluorone (H-Nu 535 from Spectra Group Ltd.) and diaryliodionium hexafluoroantimonate (SR1012 from Sartomer)(39); 5, 7-diiodo-3-butoxy-6-fluorone (H-Nu 470 from Spectra Group Ltd.) and octoxyphenylphenyl-iodonium hexafluoroantimonate (Uvacure 1600 from UCB) (60,76), and H-Nu 470 and phenyl-p-octyloxyphenyl-iodoniumhexafluoroantimonate (OPPI from Spectra Group Ltd.)(71). A single photoinitiation system, (η^6-naphthalene)(η^5-cyclopentadienyl)-iron(II) hexafluorophosphate (Irgacure 261 from Ciba Specialty Chemicals), which has absorption in visible light and generates Lewis acids upon exposure, is also demonstrated.(40,44)

To produce a clearly defined, completely open porous 3D pattern, a high pattern contrast is necessary. In multi-beam interference, the partially non-parallel polarization of three or four non-coplanar laser beams produces a non-zero background intensity ($I_0 > 0$) and, therefore, a non-zero background of generated acids ($C_0 > 0$) (Figure 5). This results in the formation of shallow patterns without fully opened holes throughout the films (Figure 6a). Although the non-zero background of the interference intensity could be minimized by fine-tuning of beam polarization, it may alter the overall symmetry of the final lattice. Thus, a chemical approach that controls the acid generation will be preferred.

In conventional photolithography, control of acid diffusion plays a pivotal role for a longer shelf life, high resolution and sharper contrast of the photoresits.(85) Base additives have been used as acid scavengers to (i) extend shelf life for low activation systems such as ketal and acetal protected poly(hydroxystyrene), (ii) improve contamination resistance for high activation resist systems, such as *t*-BOC and *t*-butyl ester resins, and (iii) reduce line width slimming and post-exposure bake sensitivity. More importantly, the base additives will limit acid diffusion and enhance chemical contrast during the exposure and bake processes, hence improving the resolution. With the addition of an appropriate amount of triethyl amine (TEA), which partially neutralizes the local photoacids generated by I_0 during exposure, we have successfully eliminated the homogeneous crosslinked background, resulting in a completely open structure throughout the film thickness (see Fig 6b and 6c).

An alternative approach is to optimize the loading of the photosensitizers.(76) Fig. 7 shows the sensitivity curve of the SU-8 photoresist as a function of 2-beam

interference exposure dose. Here, the sensitivity represents the normalized pattern contrast defined as the feature size (*d*) scaled by the feature distance (*p*). The contrast of a negative-photoresist pattern is related to the rates of both crosslinking and dissolution by the developer solution. A steeper change in crosslinking with dose energy creates a higher contrast pattern. Therefore, the slopes of the sensitivity curves in Fig. 7 suggest that the highest contrast pattern is obtained from the film loaded with 0.5 wt% photosensitizer, H-Nu 470.(76)

Due to the large porosity and long soaking time in the developer, the film delamination is nearly inevitable in 3D porous structures after development. To improve the adhesion between the porous film and the glass substrate, however, a blank resist film can be spun on glass first, flood exposed and post-exposure baked, followed by spin coating of another layer of resist film for 3D patterning.

B. Positive-tone Photoresists

Although various types of 3D photonic structures have been fabricated by multi-beam interference lithography, none of them shows complete PBG properties due to the low refractive index of polymers (e. g. SU-8, n= 1.59). To increase the refractive index contrast, polymeric photonic crystals can be used as sacrificial templates for infiltration of a higher refractive index material, followed by the removal of polymers, resulting in inversed 3D photonic crystals. Currently most 3D polymer microstructures are created in negative-tone photoresists, which form highly crosslinked 3D networks that are difficult to remove by solvent and heat below 400^{o}C. It will be advantageous to pattern 3D structures in positive-tone resists that can be easily dissolved in an organic solvent after

infiltration. A commercially available positive-tone resist, AZ5214 (Clariant International Ltd.), have been tested as a proof of concept. AZ5214 is a two-component resist system, a novolac resin as matrix and a diazonaphthoquinone as photoactive component or sensitizer. Upon exposure, the base-insoluble diazonaphthoquinone undergoes photolysis and Wolff rearrangement to form a ketene.(see Scheme 5).(48) In the presence of trace water, the ketene forms a base-soluble indenecarboxylic acid and generates a positive-tone feature. The unexposed regions can be removed by acetone. As seen in Fig. 8, a 2D hexagonal pattern was generated from three-beam interference lithography using the same optics setup reported in the literature for the fabrication of biomimetic microlens arrays in the negative-tone resist, SU-8.(44) It seems that positive-tone resists give better contrast and sharper corners than the negative-tone resists.

C. Photopolymerizable liquid resins

In addition to the solid-films of photoresists, photopolymerizable liquid resins from urethane acyrlate monomers or oligomers, and photoinitiators, have been studied for multi-beam interference lithography.(70,86) The resin becomes solidified during radical-induced photopolymerization, and the unexposed regions are washed away by alcohol. Since the liquid resin is contained in a glass cell, the thickness of the resin can be easily adjusted by cell height. 3D structures with the thickness up to 200 μm have been demonstrated using the urethane acrylate resin and a He-Cd laser (λ=442 nm). Compared to the removal of solid films, dissolution of the liquid monomers/oligomers is much faster, therefore, the developing step presumably has less effect on the integrity of the final structures. However, large shrinkage of the film after the dissolution is expected.

In addition, inhomogeneity of radical formation, the lack of control over radical diffusion, and possibility of polymerization during exposure in the liquid resins might blur the boundary of pattern, limiting the ultimate resolution of the feature size.

D. Organic-Inorganic Hybrids

As discussed above, a 3D polymer structure can be infiltrated with a higher refractive index material into the pores to obtain an inverse 3D photonic crystal. For example, an anatase titania replica can be obtained from fcc-like SU-8 pattern as shown in Fig. 9. The titania was deposited in a batch reactor under atmospheric pressure and at room temperature using titanium tetrachloride ($TiCl_4$, Aldrich) as the precursor. The sacrificial SU-8 template was removed by calcination at 500°C.

Back-filling and calcination processes often suffer from volume shrinkage that causes fracture and loss of long-range order, as well as in-complete filling. An alternative approach is to directly pattern from an organic-inorganic hybrid photoresist. For example, organosilicates can be obtained from the sol-gel reaction of 3-methacryloxypropyl trimethoxysilane with water and an acid catalyst.(87) The addition of transition metal alkoxide precursors, such as zirconium propoxide and titanium propoxide, to methacrylic acid (MA) produces photocrosslinkable organic-inorganic composites. Depending on the transition metal content, the refractive index of the hybrid can be increased to 2.0. Other titanium-containing photoresists have been synthesized from the mixture of titanium ethoxide (TE), methacrylic acid and ethylene glycol dimethacrylate (EGDMA).(62) The TE and MA produce the titania-acrylate composites while EGDMA acts as a crosslinker.

E. Holographic polymer-dispersed liquid crystals (H-PDLC)

Following the realization of 3D photonic structures, it will be interesting to incorporate active materials that will respond to the physical and chemical stimuli for tunable electro-optical devices. Moreover, the confinement of liquid crystals in 2D and 3D structures provide uniform, size- and spacing-controlled liquid crystal domains and induce orientational ordering that will lower driving voltage for reorientation of liquid crystals. One approach is to embed liquid crystals into the interstitial space of close-packed colloidal crystals.(88-90) Liquid crystals are attractive candidates because they exhibit large optical anisotropy, and their refractive index can be tuned by electrical fields or temperatures to shift the stop-bands. However, sedimentation of colloidal particles is slow (hours to days), and require multiple steps, including water evaporation, thermal annealing and back filling with liquid crystals. It could be simplified and hastened using holographic polymer-dispersed liquid crystals (H-PDLCs) based on polymerization-induced phase separation during holographic patterning. The beauty of this approach is that the liquid crystals naturally segregate to the regions of minimum intensity to phase separate from the polymers, and multi-beam interference offer a wide variety of crystal symmetries with size control in the sub-100 nm range. Similar to the conventional PDLCs(91), a photosensitive syrup consists of multi-functional photocrosslinkable monomers, such as tri-, penta- and hexa-functional urethane or acrylate oligomers, nematic liquid crystals, a visible photosensitizer, and radical initiators/co-monomers. Upon exposure to the interference of a visible light, liquid crystals are trapped in nanometer- to micron-sized droplets within a polymer matrix due

to the rapid polymerization, resulting in a periodic pattern of polymer-rich and liquid crystal-rich regions. Generally, in the absence of an electric field, the orientation of LCs induced the index mismatch between polymer matrix and liquid crystals. As the applied voltage increases, the LC directors reorient and yield the minimum index contrast, therefore, lowering the diffraction efficiency.(91,92)

1D patterns of H-PDLC have been fabricated by two-beam interference lithography as an anisotropic reflection grating(93) and a polarization grating.(94) 2D and 3D tunable H-PDLCs, such as transverse square (Fig. 10a-c)(95), fcc (Fig. 10d-f)(96), diamond-like fcc(97), and orthorhombic P lattices(Fig. 10g-i)(98) have been demonstrated using three beams, four beams, and six beams as shown in Fig. 10b, e, and h, respectively.

III. SUMMARY

Multi-beam interference lithography reviewed here offers a fast and versatile method to pattern periodic one-, two-, and three-dimensional polymer structures on the sub-micron length scale. The symmetry and shape of the "unit cell" can be conveniently controlled by varying the intensity, geometry, polarization and phase of the beams. This technique has been applied to various photoresist platforms, including UV and visible sensitive resists, negative-tone and positive-tone resists, liquid resins, organic-inorganic hybrids, and holographic polymer-dispersed liquid crystals. As a robust technique to engineer 3D porous materials, multi-beam interference may potentially impact a wide range of applications, including photonics, data storage, chemical sensors, nano- and microfludic networks and tissue engineering.

ACKNOWLEDGMENT

The authors are grateful to the students, postdoctoral researchers, and other collaborators who are involved in the work described in the review. This work is supported by the Office of Naval Research (ONR) through the MURI program, Grant # E-21-6WG-G2, the Skirkanich Chair of Innovation (SY), and the Korea Research Foundation postdoc fellowship (JHM), Grant # KRF-2005-000-10299.

Table and Figure Captions:

Table 1. A comparison of different types of 3D microfabrication techniques.

Table 2. Experimental conditions for 2D square and tetragonal lattices and the resulting lattice constants of the interference patterns. Reprinted with permission from (42). Copyright 2004 The International Society of Optical Engineering.

Table 3. Beam parameters for four-beam interference of the three-termed simple cubic, diamond-like and gyroid-like surfaces, and the resulting lattice constants. Reprinted with permission from (43). Copyright 2004 American Institute of Physics.

Scheme 1. Illustration of conventional photolithography process.

Scheme 2. Illustration of multi-beam interference lithography process.

Scheme 3. Chemical structures of photoresist, SU-8, and photoacid generator, triaryl sulfonium salt.

Scheme 4. General scheme of photosensitized cationic polymerization. Reprinted with permission from (39). Copyright 2002 American Chemical Society.

Scheme 5. Schematic illustration of the photochemistry of a diazonaphthoquinone-novolac resist system. Adapted from ref.((48))

Figure 1. Optical images of (a) two- and (b) three-beam (Reprinted with permission from (54)) interference patterns. Copyright 2003 American Physical Society.

Figure 2. 2D lattices formed from three-beam interference: (a) beam geometry in perspective, (b) beam geometry within the XY-plane showing reciprocal wave vectors, (c) resulting lattice, and (d) associated reciprocal lattice. Reprinted with permission from (42). Copyright 2004 The International Society of Optical Engineering.

Figure 3. The effect of beam polarization on a square interference pattern. The ratio of

$\mathbf{E}_1 \cdot \mathbf{E}_2$ and $\mathbf{E}_2 \cdot \mathbf{E}_3$ is (a) 2, (b) 1, and (c) 0.5, respectively.

Figure 4. The isointensity surfaces of three-termed simple cubic, diamond-like, and gyroid-like structures. Reprinted with permission from (43). Copyright 2004 American Institute of Physics.

Figure 5. Non-zero backgrounds (▨) of the light intensity and the resulting acid concentration generated in the interference pattern of non-orthogonally polarized beams. Reprinted with permission from (39). Copyright 2002 American Chemical Society.

Figure 6. Scanning electron micrographs (SEM) of micropatterned 3D polymer films. (a-c) Top view of the fcc-like structures formed in the absence (a) and in the presence (b) of TEA. (c) Cross-section of the fractured, continuously porous film shown in (b). The top surface is a (111) plane and the fractured surface is (100) plane. The scale bar is 2 μm. Reprinted with permission from (39). Copyright 2002 American Chemical Society.

Figure 7. Sensitivity curve of visible SU-8 photoresists with different loadings of photosensitizers. Reprinted with permission from (76). Copyright 2005 Elsevier Science.

Figure 8. SEM image of micropatterned AZ 5214 polymer films from three-beam interference lithography.

Figure 9. A fcc-like SU-8 photoresist pattern (inset) and its anatase titania replica. Scale bar, 5 μm.

Figure 10. Different types of 2D and 3D lattices from H-PDLCs. (a) Calculated isointensity surface, (b) arrangement of beams, and (c) SEM image of XZ-face of cylindrical cavities. Reprinted with permission from (95). Copyright 2003 American Institute of Physics. (d) Calculated isointensity surface, (e) ideal propagation vectors

within the film ($\theta \approx 63^{o}$), and (f) SEM image of polymer morphology of the fcc lattice in H-PDLC. Reprinted with permission from (96). Copyright 2003 Optical Society of America. (g) Calculated isointensity surface of YZ-plane, (h) laser beam geometry, and (i) SEM image of (100) plane after removal of the liquid crystals in orthorhombic P lattice. Scale bar, 250 nm. Reprinted with permission from (98). Copyright 2002 John Wiley & Sons, Inc.

Table 1.

Technique	Materials	Typical Dimensions (WxDxH)	Patterning Speed	Resolution	3D structures
Self-assembly(14,16)	monodispersed polymeric or inorganic particles, block copolymers	Continuous particle deposition: 100mmx100μmx10μm	seconds to days	10 nm	Periodic
Multi-beam interference lithography(36,39,42)	photosensitive polymer films (organic, hybrids)	Single exposure: 10mmx10mmx100μm	ns to seconds	300 nm	Periodic
Rapid protyping(22,23)	concentrated particle gels, colloidal gels, polymer solutions	Layer-by-layer deposition: 10mmx10mmx10mm	several mm/s	100 μm	Arbitrary
Direct-write assembly(26,27)	polyelectrolyte, concentrated colloidal gels, nanoparticle gels	Layer-by-layer writing: 10cmx10 cmx5 cm	250 μm/sec	< 1 μm	Arbitrary
Multi-photon absorption (4,30,31,35)	photosensitive monomeric liquids, polymer films, metal nanoparticles	Serial writing: 100μm x100μmx50μm	9 cm/s	120 nm	Arbitrary
GLAD (99,100)	semiconductors, metals, metal oxides, and fluorides	Rotate and step: 5cmx5cmx 8 μm	2-10Å/s	Pitch of 10's nm	chevrons, zig–zags, helical columns, superhelical

Table 2.

Lattice	The angle against z-axis, ϕ_1	Lattice constant
Square	$\phi_1 = \pi/4$, $\phi_2 = 3\pi/4$, $\phi_3 = -3\pi/4$	$\lvert\mathbf{a}_1\rvert = \lvert\mathbf{a}_2\rvert = \mathrm{a} = 0.707\lambda/\sin\theta$
Tetragonal	$\phi_1 = 0$, $\phi_2 = 2\pi/3$, $\phi_3 = -2\pi/3$	$\lvert\mathbf{a}_1\rvert = \lvert\mathbf{a}_2\rvert = \mathrm{a} = 0.667\lambda/\sin\theta$

Table 3.

Lattice	Wave vectors	Polarization Vectors	Lattice constant
Simple cubic	$k_0 = \pi / a[111]$ $k_1 = \pi / a[\bar{1}11]$ $k_2 = \pi / a[1\bar{1}1]$ $k_3 = \pi / a[11\bar{1}]$	$E_{00} = 1.00[0.0, 0.707, -0.707]$ $E_{01} = 0.632[-0.5, 0.309, -0.809]$ $E_{02} = 0.874[-0.5, 0.309, -0.898]$ $E_{03} = 2.288[-0.309, 0.809, 0.5]$	$\sqrt{3}\lambda / 2$
Diamond-like	$k_0 = \pi / a[333]$ $k_1 = \pi / a[511]$ $k_2 = \pi / a[151]$ $k_3 = \pi / a[115]$	$E_{00} = 4.897[0.612, -0.774, 0.161]$ $E_{01} = 4.000[0.25, -0.905, -0.346]$ $E_{02} = 5.789[0.346, -0.25, 0.905]$ $E_{03} = 12.94[0.905, 0.346, -0.25]$	$3\sqrt{3}\lambda / 2$
Gyroid-like	$k_0 = \pi / a[333]$ $k_1 = \pi / a[511]$ $k_2 = \pi / a[151]$ $k_3 = \pi / a[115]$	$E_{00} = 5.657[0.707, -0.707, 0]$ $E_{01} = 6.164[0.162, 0.162, -0.973]$ $E_{02} = 6.164[0.162, 0.162, -0.973]$ $E_{03} = 12.693[0.680, 0.680, -0.272]$	$3\sqrt{3}\lambda / 2$

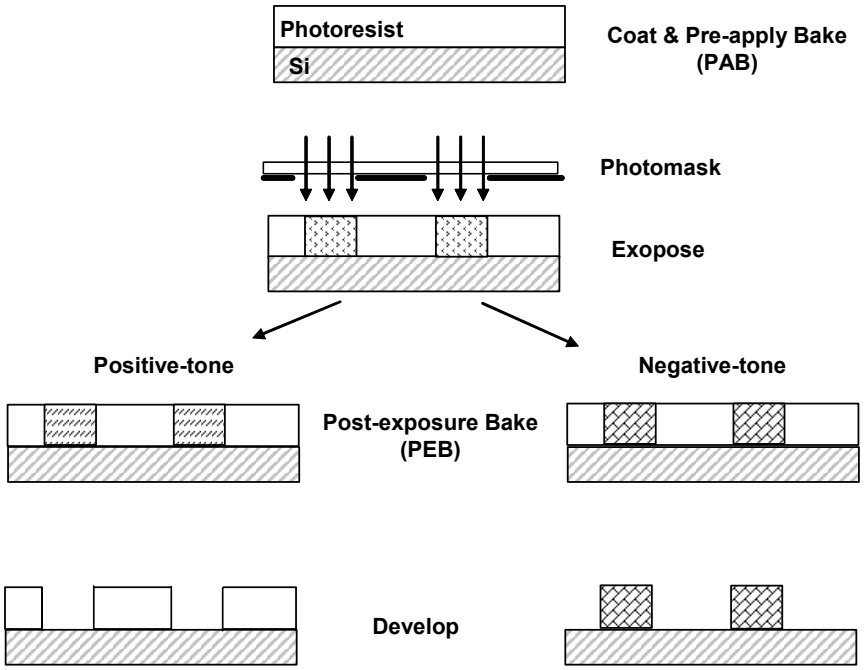
Photoresist
Si
Coat & Pre-apply Bake
(PAB)
Photomask
Exopose
Positive-tone
Negative-tone
Post-exposure Bake
(PEB)
Develop

Scheme 1.

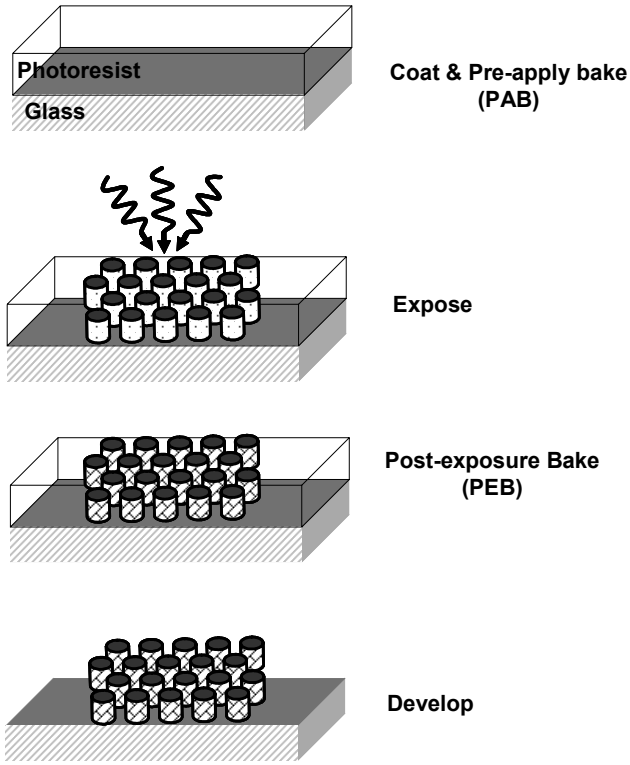
Photoresist
Glass
Coat & Pre-apply bake
(PAB)
Expose
Post-exposure Bake
(PEB)
Develop

Scheme 2.

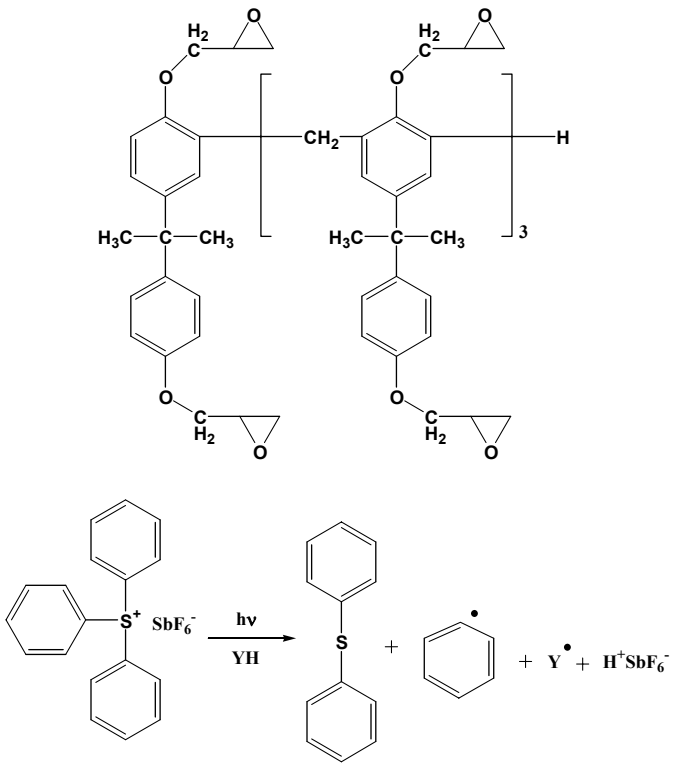

Scheme 3.

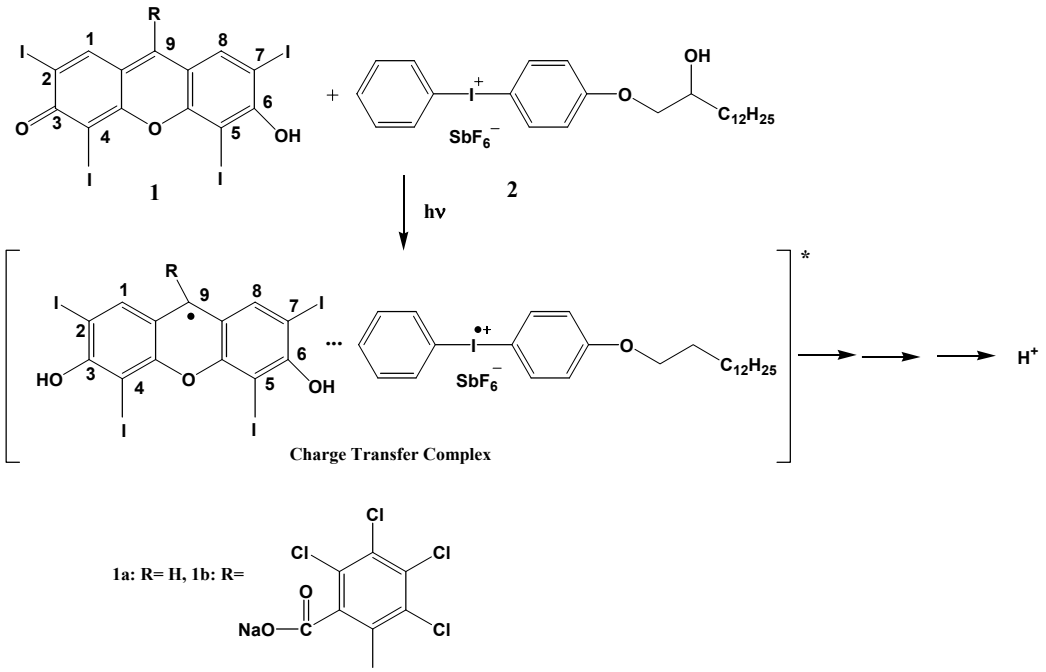

Scheme 4.

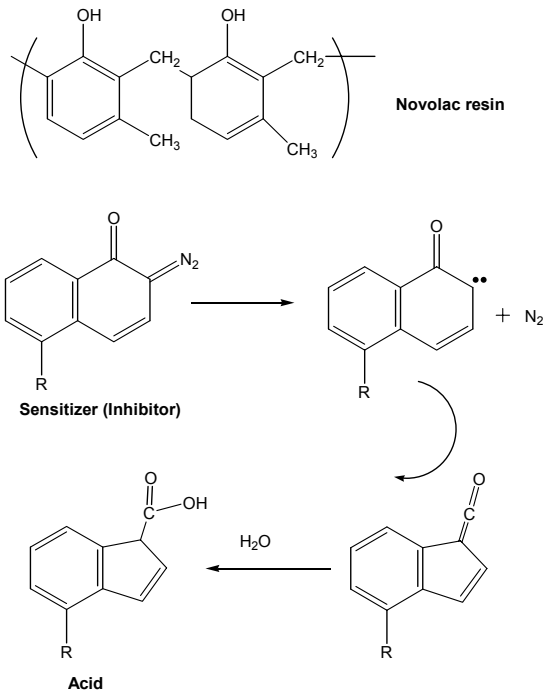
OH
OH
CH2
CH2
CH3
CH3
Novolac resin
O
N2
R
Sensitizer (Inhibitor)
O
+ N2
R
O
C
OH
R
Acid
H2O
O
C
R

Scheme 5.

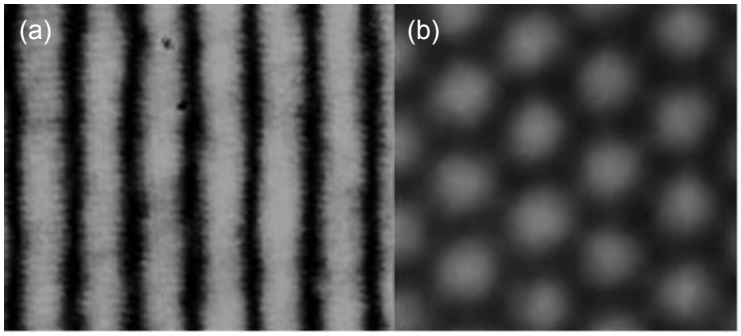

Figure 1.

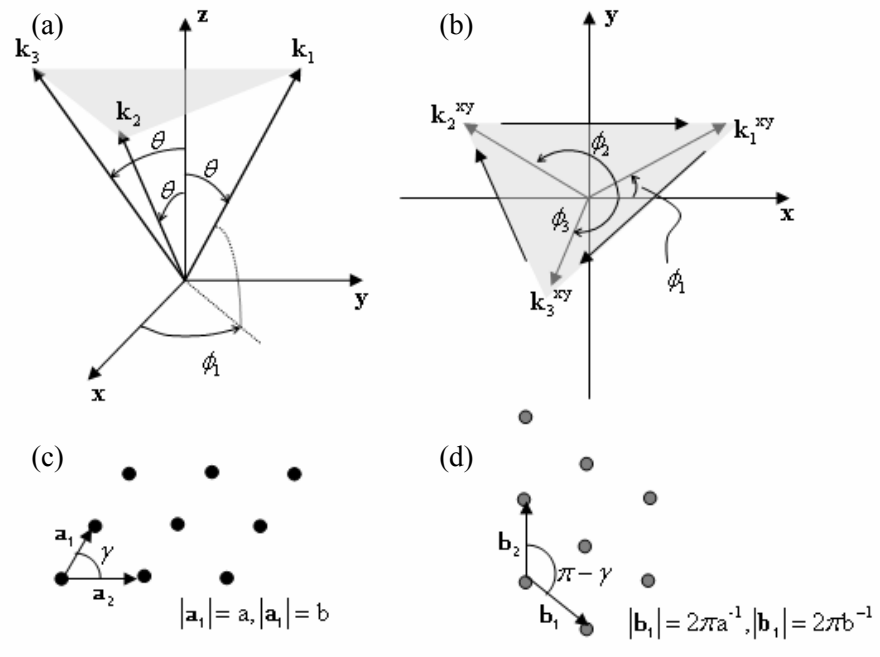
(a)
z
k3
k1
k2
θ
θ
θ
y
x
ϕ1
(b)
y
k2xy
k1xy
ϕ2
ϕ3
x
ϕ1
k3xy
(c)
a1
γ
a2
|a1| = a, |a1| = b
(d)
b2
π − γ
b1
|b1| = 2πa-1, |b1| = 2πb-1

Figure 2.

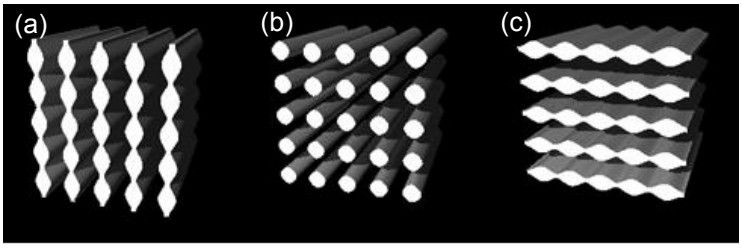

Figure 3.

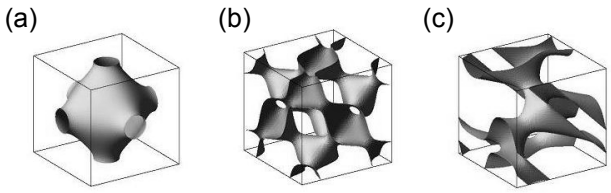

Figure 4.

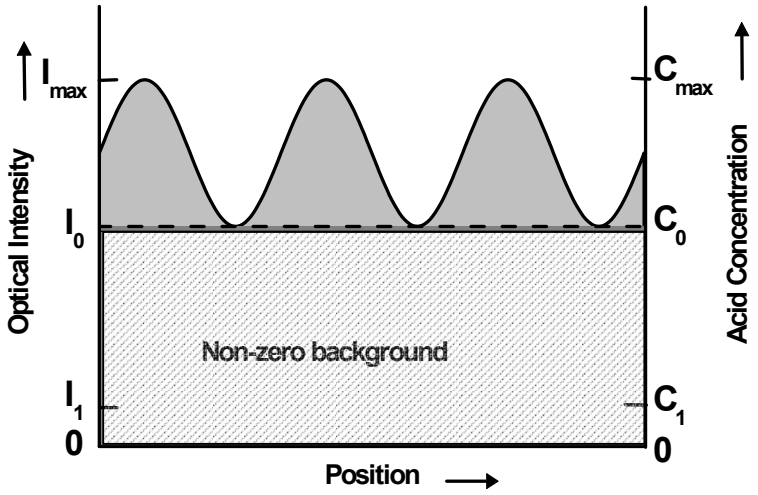
Optical Intensity
I max
I 0
I 1
0
Non-zero background
Position
C max
C 0
C 1
0
Acid Concentration

Figure 5.

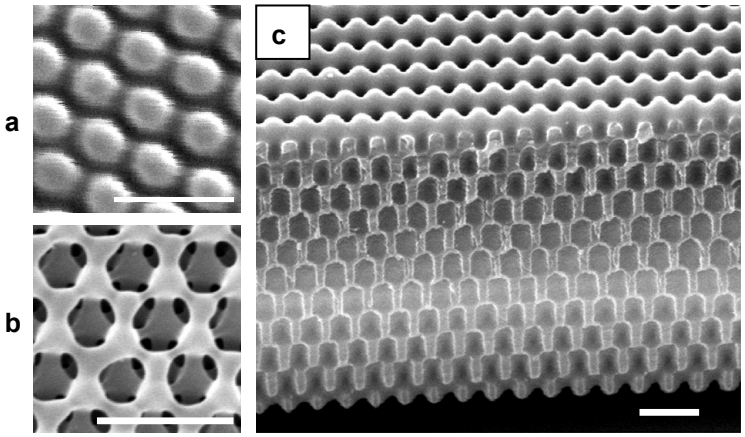

Figure 6.

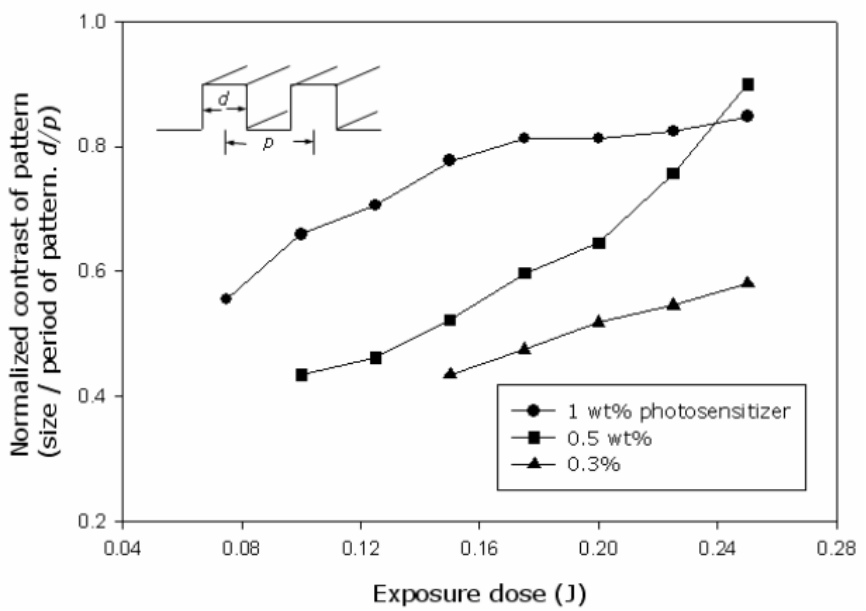
Normalized contrast of pattern
(size / period of pattern. d/p)
Exposure dose (J)
1.0
0.8
0.6
0.4
0.2
0.04
0.08
0.12
0.16
0.20
0.24
0.28
d
p
1 wt% photosensitizer
0.5 wt%
0.3%

Figure 7.

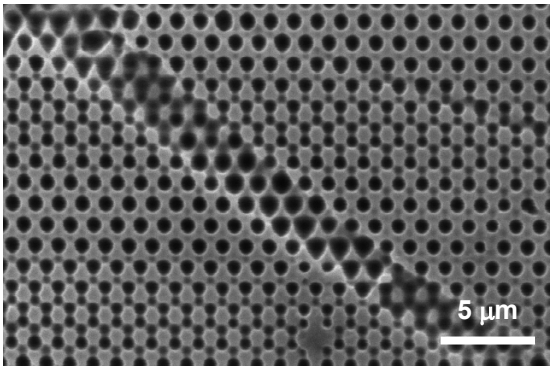

Figure 8.

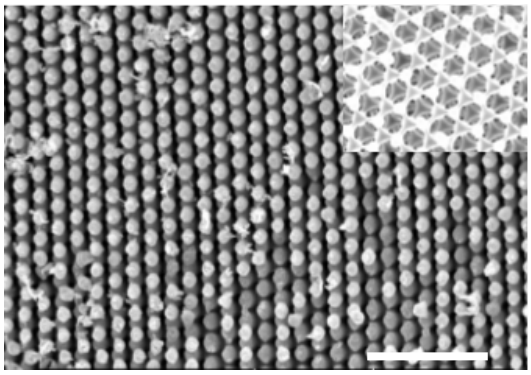

Figure 9.

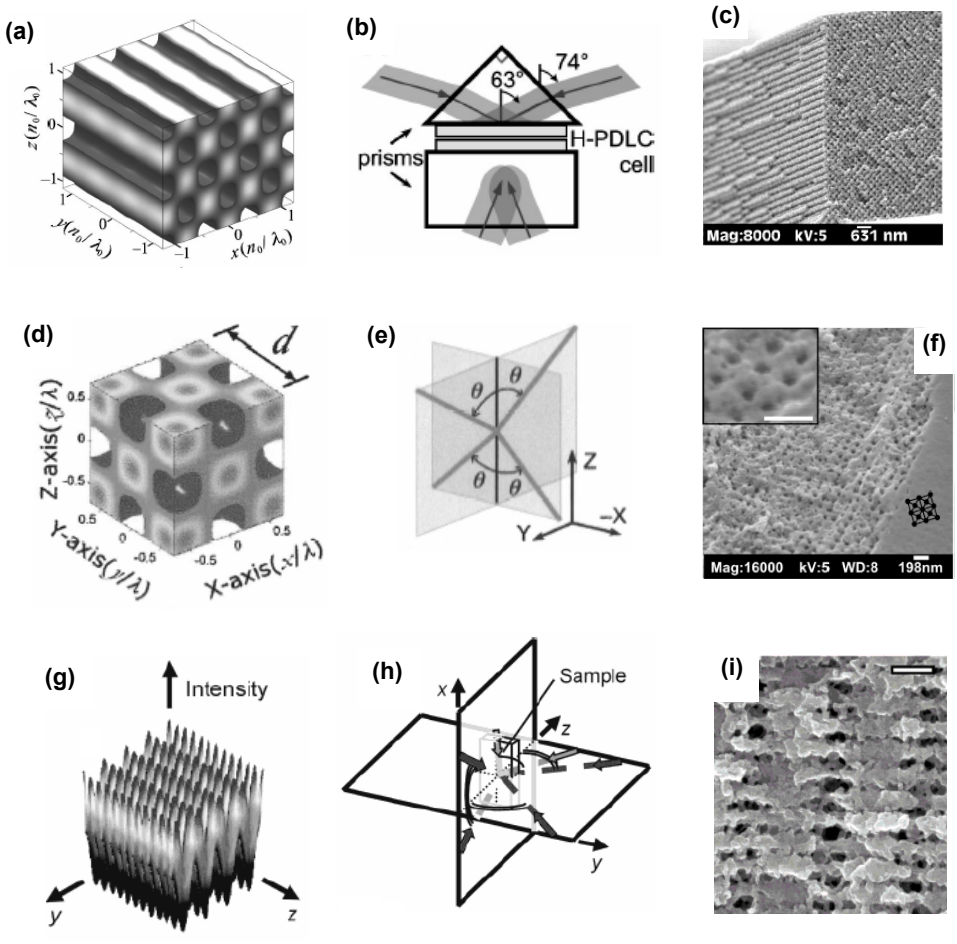
(a)
(b)
63°
74°
prisms
H-PDLC
cell
(c)
Mag:8000 kV:5 631 nm
(d)
d
Z-axis(z/λ)
Y-axis(y/λ)
X-axis(x/λ)
(e)
θ
Z
–X
Y
(f)
Mag:16000 kV:5 WD:8 198nm
(g)
Intensity
y
z
(h)
x
Sample
z
y
(i)

Figure 10.

REFERENCES

1. Polman, A.; Wiltzius, P. Materials science aspects of photonic crystals; *MRS Bulletin* **2001**, *26*(8), 608-610.
2. Li, Y. Y.; Cunin, F.; Link, J. R.; Gao, T.; Betts, R. E.; Reiver, S. H.; Chin, V.; Bhatia, S. N.; Sailor, M. J. Polymer replicas of photonic porous silicon for sensing and drug delivery applications; *Science* **2003**, *299*(5615), 2045-2047.
3. Morey, M. S.; Davidson, A.; Stucky, G. D. Silica-based, cubic mesostructures: Synthesis, characterization and relevance for catalysis; *J. Porous Mater.* **1998**, *5*(3-4), 195-204.
4. Cumpston, B. H.; Ananthavel, S. P.; Barlow, S.; Dyer, D. L.; Ehrlich, J. E.; Erskine, L. L.; Heikal, A. A.; Kuebler, S. M.; Lee, I. Y. S.; McCord-Maughon, D.; Qin, J. Q.; Rockel, H.; Rumi, M.; Wu, X. L.; Marder, S. R.; Perry, J. W. Two-photon polymerization initiators for three-dimensional optical data storage and microfabrication; *Nature* **1999**, *398*(6722), 51-54.
5. Therriault, D.; White, S. R.; Lewis, J. A. Chaotic mixing in three-dimensional microvascular networks fabricated by direct-write assembly; *Nature Mater.* **2003**, *2*(4), 265-271.
6. Abbott, A. Cell culture: Biology's new dimension; *Nature* **2003**, *424*(6951), 870-872.
7. Semino, C. E.; Merok, J. R.; Crane, G. G.; Panagiotakos, G.; Zhang, S. G. Functional differentiation of hepatocyte-like spheroid structures from putative liver progenitor cells in three-dimensional peptide scaffolds; *Differentiation* **2003**, *71*(4-5), 262-270.
8. Anders, M.; Hansen, R.; Ding, R. X.; Rauen, K. A.; Bissell, M. J.; Korn, W. M. Disruption of 3D tissue integrity facilitates adenovirus infection by deregulating the coxsackievirus and adenovirus receptor; *Proc. Nat. Acad. Sci. USA* **2003**, *100*(4), 1943-1948.
9. Qi, J.; Crawford, G. P. Holographically formed polymer dispersed liquid crystal displays; *Displays* **2004**, *25*(5), 177-186.
10. Aoki, K.; Miyazaki, H. T.; Hirayama, H.; Inoshita, K.; Baba, T.; Sakoda, K.; Shinya, N.; Aoyagi, Y. Microassembly of semiconductor three-dimensional photonic crystals; *Nature Mater.* **2003**, *2*(2), 117-121.
11. Johnson, S. G.; Joannopoulos, J. D. Three-dimensionally periodic dielectric layered structure with omnidirectional photonic band gap; *Appl. Phys. Lett.* **2000**, *77*(22), 3490-3492.

12. Lin, S. Y.; Fleming, J. G.; Hetherington, D. L.; Smith, B. K.; Biswas, R.; Ho, K. M.; Sigalas, M. M.; Zubrzycki, W.; Kurtz, S. R.; Bur, J. A three-dimensional photonic crystal operating at infrared wavelengths; *Nature* **1998**, *394*(6690), 251-253.
13. Nonogaki, S.; Ueno, T.; Ito, T. *Microlithography Fundamentals in Semiconductor Devices and Fabrication Technology*; Marcel Dekker: New York, 1998.
14. Vlasov, Y. A.; Bo, X.-Z.; Sturm, J. C.; Norris, D. J. On-chip natural assembly of silicon photonic bandgap crystals; *Nature* **2001**, *414*(6861), 289-293.
15. Colvin, V. L. From opals to optics: Colloidal photonic crystals; *MRS Bulletin* **2001**, *26*(8), 637-641.
16. Edrington, A. C.; Urbas, A. M.; DeRege, P.; Chen, C. X.; Swager, T. M.; Hadjichristidis, N.; Xenidou, M.; Fetters, L. J.; Joannopoulos, J. D.; Fink, Y.; Thomas, E. L. Polymer-based photonic crystals; *Adv. Mater.* **2001**, *13*(6), 421-425.
17. Ozin, G. A.; Yang, S. M. The race for the photonic chip: Colloidal crystal assembly in silicon wafers; *Adv. Func. Mater.* **2001**, *11*(2), 95-104.
18. Xia, Y. N.; Yin, Y. D.; Lu, Y.; McLellan, J. Template-assisted self-assembly of spherical colloids into complex and controllable structures; *Adv. Funct. Mater.* **2003**, *13*(12), 907-918.
19. Kim, S. O.; Solak, H. H.; Stoykovich, M. P.; Ferrier, N. J.; de Pablo, J. J.; Nealey, P. F. Epitaxial self-assembly of block copolymers on lithographically defined nanopatterned substrates; *Nature* **2003**, *424*(6947), 411-414.
20. Lumsdon, S. O.; Kaler, E. W.; Velev, O. D. Two-dimensional crystallization of microspheres by a coplanar AC electric field; *Langmuir* **2004**, *20*(6), 2108-2116.
21. Winkleman, A.; Gates, B. D.; McCarty, L. S.; Whitesides, G. M. Directed self-assembly of spherical particles on patterned electrodes by an applied electric field; *Adv. Mater.* **2005**, *17*(12), 1507-+.
22. Zein, I.; Hutmacher, D. W.; Tan, K. C.; Teoh, S. H. Fused deposition modeling of novel sca.old architectures for tissue engineering applications; *Biomaterials* **2002**, *23*(4), 1169-1185.
23. Landers, R.; Hubner, U.; Schmelzeisen, R.; Mulhaupt, R. Rapid prototyping of scaffolds derived from thermoreversible hydrogels and tailored for applications in tissue engineering; *Biomaterials* **2002**, *23*(23), 4437–4447.
24. Vozzi, G.; Flaim, C.; Ahluwaliaa, A.; Bhatia, S. Fabrication of PLGA scaffolds using soft lithography

and microsyringe deposition; *Biomaterials* **2003**, *24*(14), 2533-2540.

25. Chelnokov, A.; Wang, K.; Rowson, S.; Garoche, P.; Lourtioz, J. M. Near-infrared Yablonovite-like photonic crystals by focused-ion-beam etching of macroporous silicon; *Appl. Phys. Lett.* **2000**, *77*(19), 2943-2945.
26. Gratson, G. M.; Xu, M.; Lewis, J. A. Direct writing of threedimensional webs; *Nature* **2004**, *428*(6981), 386.
27. Rao, R. B.; Krafcik, K. L.; Morales, A. M.; Lewis, J. A. Microfabricated deposition nozzles for direct-write assembly of three-dimensional periodic structures; *Adv. Mater.* **2005**, *17*(3), 289-293.
28. Tang, M. D.; Golden, A. P.; Tien, J. Molding of three-dimensional microstructures of gels; *J. Am. Chem. Soc.* **2003**, *125*(43), 12988-12989.
29. Kennedy, S. R.; Brett, M. J.; Toader, O.; John, S. Fabrication of tetragonal square spiral photonic crystals; *Nano Letters* **2002**, *2*(1), 59-62.
30. Noda, S.; Tomoda, K.; Yamamoto, N.; Chutinan, A. Full three-dimensional photonic bandgap crystals at near-infrared wavelengths; *Science* **2000**, *289*(5479), 604-606.
31. Kawata, S.; Sun, H.-B.; Tanaka, T.; Takada, K. Finer features for functional microdevices; *Nature* **2001**, *412*(6848), 697-698.
32. Stellacci, F.; Bauer, C. A.; Meyer-Friedrichsen, T.; Wenseleers, W.; Marder, S. R.; Perry, J. W. Ultrabright supramolecular beacons based on the self-assembly of two-photon chromophores on metal nanoparticles; *J. Am. Chem. Soc.* **2003**, *125*(2), 328-329.
33. Wu, P. W.; Cheng, W.; Martini, I. B.; Dunn, B.; Schwartz, B. J.; Yablonovitch, E. Two-photon photographic production of three-dimensional metallic structures within a dielectric matrix; *Adv. Mater.* **2000**, *12*(19), 1438-1441.
34. Zhou, W. H.; Kuebler, S. M.; Braun, K. L.; Yu, T. Y.; Cammack, J. K.; Ober, C. K.; Perry, J. W.; Marder, S. R. An efficient two-photon-generated photoacid applied to positive-tone 3D microfabrication; *Science* **2002**, *296*(5570), 1106-1109.
35. Deubel, M.; Von Freymann, G.; Wegener, M.; Pereira, S.; Busch, K.; Soukoulis, C. M. Direct laser writing of three-dimensional photonic-crystal templates for telecommunications; *Nature Mater.* **2004**, *3*(7), 444-447.

36. Campbell, M.; Sharp, D. N.; Harrison, M. T.; Denning, R. G.; Turberfield, A. J. Fabrication of photonic crystals for the visible spectrum by holographic lithography; *Nature* **2000**, *404*(6773), 53-56.
37. Divliansky, I.; Mayer, T. S.; Holliday, K. S.; Crespi, V. H. Fabrication of three-dimensional polymer photonic crystal structures using single diffraction element interference lithography; *Appl. Phys. Lett.* **2003**, *82*(11), 1667-1669.
38. Divliansky, I. B.; Shishido, A.; Khoo, I. C.; Mayer, T. S.; Pena, D.; Nishimura, S.; Keating, C. D.; Mallouk, T. E. Fabrication of two-dimensional photonic crystals using interference lithography and electrodeposition of CdSe; *Appl. Phys. Lett.* **2001**, *79*(21), 3392-3394.
39. Yang, S.; Megens, M.; Aizenberg, J.; Wiltzius, P.; Chaikin, P. M.; Russel, W. B. Creating periodic three-dimensional structures by multibeam interference of visible laser; *Chem. Mater.* **2002**, *14*(7), 2831-2833.
40. Wang, X.; Xu, J. F.; Su, H. M.; Zeng, Z. H.; Chen, Y. L.; Wang, H. Z.; Pang, Y. K.; Tam, W. Y. Three-dimensional photonic crystals fabricated by visible light holographic lithography; *Appl. Phys. Lett.* **2003**, *82*(14), 2212-2214.
41. Sharp, D. N.; Turberfield, A. J.; Denning, R. G. Holographic photonic crystals with diamond symmetry; *Phys. Rev. B* **2003**, *68*(20), 205102.
42. Escuti, M. J.; Crawford, G. P. Holographic photonic crystals; *Opt. Eng.* **2004**, *43*(9), 1973-1987.
43. Ullal, C. K.; Maldovan, M.; Thomas, E. L.; Chen, G.; Han, Y.-J.; Yang, S. Photonic crystals through holographic lithography: simple cubic, diamond-like and gyroid-like structures; *Appl. Phys. Lett.* **2004**, *84*(26), 5434-5436.
44. Yang, S.; Chen, G.; Megens, M.; Ullal, C. K.; Han, Y. J.; Rapaport, R.; Thomas, E. L.; Aizenberg, J. Functional biomimetic microlens arrays with integrated pores; *Adv. Mater.* **2005**, *17*(4), 435-438.
45. Fernandez, A.; Bedrossian, P. J.; Baker, S. L.; Vernon, S. P.; Kania, D. R. Magnetic force microscopy of single-domain cobalt dots patterned using interference lithography; *IEEE Trans. Magnet.* **1996**, *32*(5), 4472-4474.
46. Vogelaar, L.; Nijdam, W.; van Wolferen, H.; de Ridder, R. M.; Segerink, F. B.; Fluck, E.; Kuipers, L.; van Hulst, N. F. Large area photonic crystal slabs for visible light with waveguiding defect structures: Fabrication with focused ion beam assisted laser interference lithography; *Adv. Mater.* **2001**, *13*(20),

1551-1554.

47. Kang, J. W.; Kim, M. J.; Kim, J. P.; Yoo, S. J.; Lee, J. S.; Kim, D. Y.; Kim, J. J. Polymeric wavelength filters fabricated using holographic surface relief gratings on azobenzene-containing polymer films; *Appl. Phys. Lett.* **2003**, *82*(22), 3823-3825.
48. Thompson, L. F.; Willson, C. G.; Bowden, M. J. *Introduction to microlithography*; 2 nd ed.; American Chemical Society: Washington, DC, 1994.
49. Petsas, K. I.; Coates, A. B.; Grynberg, G. Crystallography Of Optical Lattices; *Phys. Rev. A* **1994**, *50*(6), 5173-5189.
50. Yuan, L.; Wang, G. P.; Huang, X. K. Arrangements of four beams for any Bravais lattice; *Opt. Lett.* **2003**, *28*(19), 1769-1771.
51. Cai, L. Z.; Yang, X. L.; Liu, Q.; Wang, Y. R. What kind of Bravais lattices can be made by the interference of four umbrellalike beams? *Opt. Comm.* **2003**, *224*(4-6), 243-246.
52. Cai, L. Z.; Yang, X. L.; Wang, Y. R. Formation of three-dimensional periodic microstructures by interference of four noncoplanar beams; *J. Opt. Soc. Am. A* **2002**, *19*(11), 2238-2244.
53. Cai, L. Z.; Yang, X. L.; Wang, Y. R. All fourteen Bravais lattices can be formed by interference of four noncoplanar beams; *Opt. Lett.* **2002**, *27*(11), 900-902.
54. Su, H. M.; Zhong, Y. C.; Wang, X.; Zheng, X. G.; Xu, J. F.; Wang, H. Z. Effects of polarization on laser holography for microstructure fabrication; *Phys. Rev. E* **2003**, *67*(5), 056619.
55. Ullal, C. K.; Maldovan, M.; Wohlgemuth, M.; Thomas, E. L. Triply periodic bicontinuous structures through interference lithography: a level-set approach; *J. Opt. Soc. Am. A* **2003**, *20*(5), 948-954.
56. Grynberg, G.; Lounis, B.; Verkerk, P.; Courtois, J. Y.; Salomon, C. Quantized Motion of Cold Cesium Atoms in 2-Dimensional and 3- Dimensional Optical Potentials; *Phys. Rev. Lett.* **1993**, *70*(15), 2249-2252.
57. Dufresne, E. R.; Spalding, G. C.; Dearing, M. T.; Sheets, S. A.; Grier, D. G. Computer-generated holographic optical tweezer arrays; *Rev. Sci. Instr.* **2001**, *72*(3), 1810-1816.
58. Curtis, J. E.; Koss, B. A.; Grier, D. G. Dynamic holographic optical tweezers; *Opt. Comm.* **2002**, *207*(1-6), 169-175.
59. Ladavac, K.; Grier, D. G. Microoptomechanical pumps assembled and driven by holographic optical

vortex arrays; *Opt. Exp.* **2004**, *12*(6), 1144-1149.

60. Moon, J. H.; Yang, S. M.; Pine, D. J.; Chang, W. S. Multiple-exposure holographic lithography with phase shift; *Appl. Phys. Lett.* **2004**, *85*(18), 4184-4186.
61. Berger, V.; GauthierLafaye, O.; Costard, E. Fabrication of a 2D photonic bandgap by a holographic method; *Electron. Lett.* **1997**, *33*(5), 425-426.
62. Shishido, A.; Diviliansky, I. B.; Khoo, I. C.; Mayer, T. S.; Nishimura, S.; Egan, G. L.; Mallouk, T. E. Direct fabrication of two-dimensional titania arrays using interference photolithography; *Appl. Phys. Lett.* **2001**, *79*(20), 3332-3334.
63. Zaidi, S. H.; Brueck, S. R. J. Multiple-Exposure Interferometric Lithography; *J. Vac. Sci. Technol. B* **1993**, *11*(3), 658-666.
64. Gigli, G.; Rinaldi, R.; Turco, C.; Visconti, P.; Cingolani, R.; Cacialli, F. Holographic nanopatterning of the organic semiconductor poly(p-phenylene vinylene); *Appl. Phys. Lett.* **1998**, *73*(26), 3926-3928.
65. Solak, H. H.; David, C.; Gobrecht, J.; Wang, L.; Cerrina, F. Multiple-beam interference lithography with electron beam written gratings; *J. Vac. Sci. Technol. B* **2002**, *20*(6), 2844-2848.
66. Pang, L.; Nakagawa, W.; Fainman, Y. Fabrication of two-dimensional photonic crystals with controlled defects by use of multiple exposures and direct write; *Appl. Opt.* **2003**, *42*(27), 5450-5456.
67. Visconti, P.; Turco, C.; Rinaldi, R.; Cingolani, R. Nanopatterning of organic and inorganic materials by holographic lithography and plasma etching; *Microelec. Eng.* **2000**, *53*(1-4), 391-394.
68. Yablonovitch, E.; Gmitter, T. J. Photonic Band-Structure - the Face-Centered-Cubic Case; *Phys. Rev. Lett.* **1989**, *63*(18), 1950-1953.
69. Joannopoulos, J. D.; Meade, R. D.; Winn, J. N. *Photonic Crystals*; Princeton University Press: Princeton, NJ, 1995.
70. Shoji, S.; Kawata, S. Photofabrication of three-dimensional photonic crystals by multibeam laser interference into a photopolymerizable resin; *Appl. Phys. Lett.* **2000**, *76*(19), 2668-2670.
71. Lin, Y.; Herman, P. R.; Darmawikarta, K. Design and holographic fabrication of tetragonal and cubic photonic crystals with phase mask: toward the mass-production of three-dimensional photonic crystals; *Appl. Phys. Lett.* **2005**, *86*(7), 071117.
72. Miklyaev, Y. V.; Meisel, D. C.; Blanco, A.; von Freymann, G.; Busch, K.; Koch, W.; Enkrich, C.;

Deubel, M.; Wegener, M. Three-dimensional face-centered-cubic photonic crystal templates by laser holography: fabrication, optical characterization, and band-structure calculations; *Appl. Phys. Lett.* **2003**, *82*(8), 1284-1286.

73. Toader, O.; Chan, T. Y. M.; John, S. Photonic band gap architectures for holographic lithography; *Phys. Rev. Lett.* **2004**, *92*(4), 043905.
74. Maldovan, M.; Thomas, E. L. Diamond-structured photonic crystals; *Nature Mater.* **2004**, *3*(9), 593-600.
75. Wohlgemuth, M.; Yufa, N.; Hoffman, J.; Thomas, L. E. Triply periodic bicontinuous cubic microdomain morphologies by symmetries; *Macromolecules* **2001**, *34*(17), 6083-6089.
76. Moon, J. H.; Small, A.; Yi, G. R.; Lee, S. K.; Chang, W. S.; Pine, D. J.; Yang, S. M. Patterned polymer photonic crystals using soft lithography and holographic lithography; *Syn. Metals* **2005**, *148*(1), 99-102.
77. Lee, K. Y.; LaBianca, N.; Rishton, S. A.; Zolgharnain, S.; Gelorme, J. D.; Shaw, J.; Chang, T. H. P. Micromachining applications of a high resolution ultrathick photoresist; *J. Vac. Sci. Technol. B* **1995**, *13*(6), 3012-3016.
78. Shaw, J. M.; Gelorme, J. D.; LaBianca, N. C.; Conley, W. E.; Holmes, S. J. Negative photoresists for optical lithography; *IBM J. Res. Dev.* **1997**, *41*(1-2), 81.
79. Rajaraman, S. K.; Mowers, W. A.; Crivello, J. V. Interaction of epoxy and vinyl ethers during photoinitiated cationic polymerization; *J. Polym. Sci. A-Polym. Chem.* **1999**, *37*(21), 4007-4018.
80. Boey, F.; Rath, S. K.; Ng, A. K.; Abadie, M. J. M. Cationic UV cure kinetics for multifunctional epoxies; *J. Appl. Polym. Sci.* **2002**, *86*(2), 518-525.
81. Bi, Y. B.; Neckers, D. C. A Visible-Light Initiating System For Free-Radical Promoted Cationic Polymerization; *Macromolecules* **1994**, *27*(14), 3683-3693.
82. Hua, Y. J.; Crivello, J. V. Development of polymeric photosensitizers for photoinitiated cationic polymerization; *Macromolecules* **2001**, *34*(8), 2488-2494.
83. Crivello, J. V.; Lam, J. H. W. Dye-sensitized photoinitiated Cationic Polymerization; *J. Polym. Sci: Polym. Chem. Ed.* **1978**, *16*(10), 2441-2451.
84. Crivello, J. V.; Sangermano, M. Visible and long-wavelength photoinitiated cationic polymerization; *J. Polym. Sci. A-Polym. Chem.* **2001**, *39*(3), 343-356.

85. Hinsberg, W.; Houle, F. A.; Sanchez, M.; Morrison, M.; Wallraff, G.; Larson, C.; Hoffnagle, J.; Brock, P.; Breyta, G.; Effect of resist components on image spreading during postexposure bake of chemically amplified resists; In *Advances in Resist Technology and Processing XVII*; California; Houlihan, F. M., Ed.; The International Society for Optical Engineering:2000; p 148.

86. Shoji, S.; Sun, H. B.; Kawata, S. Photofabrication of wood-pile three-dimensional photonic crystals using four-beam laser interference; *Appl. Phys. Lett.* **2003**, *83*(4), 608-610.

87. Saravanamuttu, K.; Blanford, C. F.; Sharp, D. N.; Dedman, E. R.; Turberfield, A. J.; Denning, R. G. Sol-gel organic-inorganic composites for 3-D holographic lithography of photonic crystals with submicron periodicity; *Chem. Mater.* **2003**, *15*(12), 2301-2304.

88. Yoshino, K.; Shimoda, Y.; Kawagishi, Y.; Nakayama, K.; Ozaki, M. Temperature tuning of the stop band in transmission spectra of liquid-crystal infiltrated synthetic opal as tunable photonic crystal; *Appl. Phys. Lett.* **1999**, *75*(7), 932-934.

89. Kang, D.; Maclennan, J. E.; Clark, N. A.; Zakhidov, A. A.; Baughman, R. H. Electro-optic behavior of liquid-crystal-filled silica opal photonic crystals: Effect of liquid-crystal alignment; *Phys. Rev. Lett.* **2001**, *86*(18), 4052-4055.

90. Mach, P.; Wiltzius, P.; Megens, M.; Weitz, D. A.; Lin, K. H.; Lubensky, T. C.; Yodh, A. G. Electro-optic response and switchable Bragg diffraction for liquid crystals in colloid-templated materials; *Phys. Rev. E* **2002**, *65*(3), 031720.

91. Bunning, T. J.; Natarajan, L. V.; Tondiglia, V. P.; Sutherland, R. L. Holographic polymer-dispersed liquid crystals (H-PDLCs); *Ann. Rev. Mater. Sci.* **2000**, *30*(1), 83-115.

92. Boiko, Y.; Eakin, J.; Vedrine, J.; Crawford, G. P. Polarization-selective switching in holographically formed polymer dispersed liquid crystals; *Optics Letters* **2002**, *27*(19), 1717-1719.

93. Sutherland, R. L.; Tondiglia, V. P.; Natarajan, L. V.; Bunning, T. J. Evolution of anisotropic reflection gratings formed in holographic polymer-dispersed liquid crystals; *Appl. Phys. Lett.* **2001**, *79*(10), 1420-1422.

94. Kawatsuki, N.; Hasegawa, T.; Ono, H.; Tamoto, T. Formation of polarization gratings and surface relief gratings in photocrosslinkable polymer liquid crystals by polarization holography; *Adv. Mater.* **2003**, *15*(12), 991-994.

95. Escuti, M. J.; Qi, J.; Crawford, G. P. Two-dimensional tunable photonic crystal formed in a liquid-crystal/polymer composite: Threshold behavior and morphology; *Appl. Phys. Lett.* **2003**, *83*(7), 1331-1333.

96. Escuti, M. J.; Qi, J.; Crawford, G. P. Tunable face-centered-cubic photonic crystal formed in holographic polymer dispersed liquid crystals; *Opt. Lett.* **2003**, *28*(7), 522-524.

97. Escuti, M. J.; Crawford, G. P. Mesoscale three dimensional lattices formed in polymer dispersed liquid crystals: A diamond-like face centered cubic; *Mol. Cryst. Liq. Cryst.* **2004**, *421*(23-36.

98. Tondiglia, V. P.; Natarajan, L. V.; Sutherland, R. L.; Tomlin, D.; Bunning, T. J. Holographic formation of electro-optical polymer-liquid crystal photonic crystals; *Adv. Mater.* **2002**, *14*(3), 187-191.

99. Robbie, K.; Brett, M. J. Sculptured thin films and glancing angle deposition: Growth mechanics and applications; *J. Vac. Sci. Technol. A* **1997**, *15*(3), 1460-1465.

100. Robbie, K.; Sit, J. C.; Brett, M. J. Advanced techniques for glancing angle deposition; *J. Vac. Sci. Technol. B* **1998**, *16*(3), 1115-1122.